Environmental Science & Technology

Article

pubs.acs.org/est

Ups and Downs in the Ocean: Effects of Biofouling on Vertical Transport of Microplastics

Merel Kooi,*[,†] Egbert H. van Nes,[†] Marten Scheffer,[†] and Albert A. Koelmans[†,‡]

[†]Aquatic Ecology and Water Quality Management Group, Department of Environmental Sciences, Wageningen University & Research, P.O. Box 47, 6700 AA Wageningen, The Netherlands

[‡]Wageningen Marine Research, P.O. Box 68, 1970 AB IJmuiden, The Netherlands

Supporting Information

ABSTRACT: Recent studies suggest size-selective removal of small plastic particles from the ocean surface, an observation that remains unexplained. We studied one of the hypotheses regarding this size-selective removal: the formation of a biofilm on the microplastics (biofouling). We developed the first theoretical model that is capable of simulating the effect of biofouling on the fate of microplastic. The model is based on settling, biofilm growth, and ocean depth profiles for light, water density, temperature, salinity, and viscosity. Using realistic parameters, the model simulates the vertical transport of small microplastic particles over time, and predicts that the particles either float, sink to the ocean floor, or oscillate vertically, depending on the size and density of the particle. The predicted size-dependent vertical movement of microplastic particles results in a maximum concentration at intermediate depths. Consequently, relatively low abundances of small particles are predicted at the ocean surface, while at the same time these small particles may never reach the ocean floor. Our results hint at the fate of "lost" plastic in the ocean, and provide a start for predicting risks of exposure to microplastics for potentially vulnerable species living at these depths.

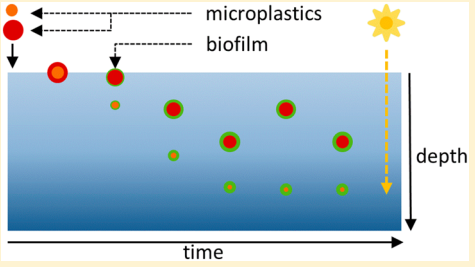

INTRODUCTION

Plastic waste entering the oceans was estimated between 4.8 and 12.7 million metric tons for 2010, and these amounts are expected to increase 1 order of magnitude by 2025.[1] This plastic debris will fragment to smaller particles due to photodegradation, physical erosion, or biodegradation.[2] Consequently, microplastics, defined as plastic particles <5 mm, are numerically more abundant than larger plastic debris, both at the sea surface and in the water column.[3−6] Microplastics can, among others, be ingested by detritivores, deposit feeders, filter feeders, and zooplankton.[7−10] Ingestion may cause chemical leaching and blockage or damage of digestive tracts, resulting in satiation, starvation, and physical deterioration of organisms.[7]

Because of the fragmentation of larger plastic, it is expected that the number of particles in the ocean increases exponentially with decreasing size.[6] However, a size-dependent lack of small particles was observed at the ocean surface, suggesting that particles smaller than 1 mm are somehow "lost".[6,11] While microplastic amounts have accumulated in the pelagic zone,[12] microplastic fate below the ocean surface remains largely unknown.[6,13] There are several hypotheses for the removal of these smaller particles, such as ingestion by marine organisms,[6] vertical transport caused by wind mixing,[14] the accumulation of organisms on plastics (biofouling) followed by settling,[6,15] fast degradation to very small particles ("nanofragmentation")[6] or a combination thereof. Here we study whether the biofouling hypothesis can explain the fate of the "lost" plastics.

Biofouling is defined as the accumulation of organisms on submerged surfaces and affects the hydrophobicity and buoyancy of plastic.[15−19] When the density of a particle with biofilm exceeds seawater density, it starts to settle.[15,18] As seawater density gradually increases with depth, the particle can be expected to stay suspended at the depth were its density equals seawater density.[6,15] It has been hypothesized that the depths at which the particles are suspended might be equal to the pycno- and thermocline depth.[15] It is also possible that particles sink deeper as several studies indicate the presence of microplastics on the ocean floor, although the transport mechanisms remain unknown.[20−22] Biofouling occurs within days, and within weeks algal fouling communities are formed on the plastic surfaces.[15,17,23] Plastics can start sinking within 2 weeks, the time depending on particle size, type, shape, roughness, and environmental conditions.[23] Ye and Andrady (1991) report sinking of plastics within 7 weeks, but also indicate that defouling occurs quickly after particle submersion.[15] Defouling can be the result of light limitation, grazing, or dissolution of carbonates in acid waters.[6,15] Fouling also occurs under submerged conditions, but with different algae species and at a slower rate.[15,17]

The development of dynamic models for biofouling and microplastic settling is essential in order to predict the vertical

Received: September 19, 2016
Revised: June 14, 2017
Accepted: June 14, 2017
Published: June 14, 2017

DOI: 10.1021/acs.est.6b04702
Environ. Sci. Technol. 2017, 51, 7963−7971

distribution of microplastics. The above shows that there are several empirical studies addressing biofouling, however, deterministic quantitative frameworks that are capable of simulating the effects of biofouling on the vertical distribution of microplastics are lacking. Modeling fouled plastic movement from a theoretical point of view is useful in order to evaluate the different factors and processes influencing microplastic biofouling and the associated sinking through scenario analysis. In the present study we provide the first theoretical model that simulates the effect of biofouling on the settling of microplastics. We modeled particles ranging between 10 mm and 0.1 μm in radius, and for convenience refer to all these particles as "microplastics". We present model simulations that show the effect of particle size, particle type (density), and oceanographic variables on the fouling of plastic by attachment of algae and subsequent settling. To explain the observed systems behavior, selected additional calculations are performed. These calculations include assessment of the dependence of the model outcome to variability in some of the key parameters.

METHODS

Modeling the Effect of Biofouling on the Vertical Transport of Microplastics. The model simulates settling or rising of microplastic particles, dependent on density differences between the composite particles and seawater and uses well-established concepts and parametrizations for all of its components. The composite particle density was determined by algae attachment, growth, respiration, and mortality. Settling of plastic particles over depth z was modeled as a function of the settling velocity V_s (m s^{-1}).

$$\frac{dz}{dt} = V_s(z, t) \tag{1}$$

Microplastic particles come in many shapes. Hence, the settling velocity V_s was calculated using a modification of the Stokes equation, provided by Dietrich (1982).[24] This equation can be applied to both spherical and nonspherical particles by using an equivalent spherical diameter[24] and was recently verified for microplastics, using settling data for spherical, pristine microplastic particles:[25]

$$V_s(z, t) = -\left(\frac{\rho_{tot} - \rho_{sw,z}}{\rho_{sw,z}} g\omega_* \nu_{sw,z}\right)^{1/3} \tag{2}$$

in which ρ_{tot} is the density of the plastic particle with biofilm (kg m^{-3}), $\rho_{sw,z}$ is the seawater density at depth z (kg m^{-3}), $\nu_{sw,z}$ is the kinematic viscosity of the seawater (m^2 s^{-1}), g is the gravitational acceleration (m s^{-2}) and ω_* is the dimensionless settling velocity.[24] The dimensionless settling velocity ω_* is a function of the dimensionless particle diameter D_*. The dimensionless settling velocity was calculated as[24]

$$\omega_* = 1.74 \times 10^{-4} D_*^2 \quad \text{for} \quad D_* < 0.05 \tag{3}$$

$$\log(\omega_*) = -3.76715 + 1.92944 \log D_* - 0.09815(\log D_*)^{2.0} - 0.00575(\log D_*)^{3.0} + 0.00056(\log D_*)^{4.0} \quad \text{for} \quad 0.05 \geq D_* \geq 5 \times 10^9$$

The dimensionless particle diameter was calculated from the equivalent spherical diameter D_n (m):[24]

$$D_* = \frac{(\rho_{tot} - \rho_{sw,z}) g D_n^3}{\rho_{sw,z} \nu_{sw,z}^2} \tag{4}$$

In our heuristic and conceptual model approach, the "average" plastic particle was assumed to be spherical, and the biofilm was assumed to be homogeneously distributed over the particle. The density of the plastic particle with biofilm could therefore be expressed as

$$\rho_{tot}(z, t) = \frac{r_{pl}^3 \rho_{pl} + [(r_{pl} + t_{bf})^3 - r_{pl}^3]\rho_{bf}}{(r_{pl} + t_{bf})^3} \tag{5}$$

in which the total density, ρ_{tot} (kg m^{-3}), was calculated from the particle radius r_{pl} (m), the biofilm thickness t_{bf} (m) and the biofilm and plastic density; ρ_{bf} and ρ_{pl}, respectively (kg m^{-3}). It was assumed that the biofilm density exceeds seawater density because several studies indicate the sinking of buoyant plastics when fouled.[15,23] Biofilm thickness was calculated as the difference between the radius of the total biofouled particle and the radius of the plastic particle, using the following equations.

$$t_{bf} = \sqrt[3]{V_{tot}\frac{3}{4\pi}} - r_{pl} \tag{6}$$

$$V_{tot} = V_{bf} + V_{pl} \tag{7}$$

$$V_{pl} = \frac{4}{3}\pi r_{pl}^3 \tag{8}$$

$$\theta_{pl} = 4\pi r_{pl}^2 \tag{9}$$

The volumes, V_{tot}, V_{bf}, and V_{pl}, are the total, biofilm, and plastic volume, respectively (m^3). θ_{pl} (m^2) is the surface area of the plastic particle. Although algae and bacillus bacteria are the most common species found in biofilms,[26] our basic model contains only algae. After all, the weight of bacteria is much smaller than the weight of algae, whereas the number of bacteria in biofilms is less than twice as much as the number of algae.[26] Biofilm volume was calculated using the volume of algae cells, V_A (m^3), the number of attached algae, A (no. m^{-2}), and the plastic surface area:

$$V_{bf} = (V_A A)\theta_{pl} \tag{10}$$

In case the plastic volume is smaller than the algae cell volume, the algae biomass is also calculated to be homogeneously distributed around the plastic particle. Attached algal growth, dA/dt, was dynamically modeled as

$$\frac{dA}{dt} = \frac{\beta_A A_A}{\theta_{pl}} + \mu_A(T, I)A - m_A A - Q_{10}^{(T-20)/10} R_{20} A \tag{11}$$

in which the first term models fouling through collision of algae with the plastic particles,[27] the second term calculates light and temperature limited growth,[28] the third term accounts for (grazing) mortality,[28] and the last term quantifies respiration.[29] Hereafter, we detail the calculations of the four terms successively.

Collision of the particle with algae (eq 11, term 1) is dependent on the ambient algae concentration, A_A (no. m^{-3}), and the encounter kernel rate, β_A (m^3 s^{-1}). Data on concentrations of algae over depth do not exist; however, it has been reported that chlorophyll-a concentrations vary with depth.[30] Therefore, algae concentrations were calculated from

DOI: 10.1021/acs.est.6b04702
Environ. Sci. Technol. 2017, 51, 7963−7971

an imposed chlorophyll-a profile, using the chlorophyll-a/carbon[31] and carbon/algae cell ratio.[32] A fixed conversion factor for the carbon/algae cells ratio was used (mg C cell^{-1}), and for the conversion of chlorophyll-a/carbon ratio, in mg *Chl a* (mg C)$^{-1}$, we used the following temperature and light-dependent equation:[31]

$$Chl\ a\text{: C} = 0.003 + 1.0154\ e^{0.050T}\ e^{-0.059I_z/10^6}\mu' \quad (12)$$

where nutrients are assumed to be sufficiently available for the algae.

We used a modification of a Gaussian equation to model the vertical chlorophyll-a profile, which is a well-accepted method in oceanography:[30,33]

$$Chl(z) = \frac{Chl\ a\ (z)}{\overline{Chl\ a}_{Z_{base}}} = C_b - sz + C_{max}\ e^{-((z-Z_{max})/\Delta z)^2} \quad (13)$$

in which $Chl\ (Z)$ is the normalized chlorophyll concentration at depth z, C_b is the normalized surface concentration, s is the normalized slope, C_{max} is the normalized maximum concentration, Z_{max} (m) is the depth at which the maximum concentration can be found and Δz (m) is the width of the peak. $\overline{Chl\ a}_{z_{base}}$ is the average chlorophyll-a concentration of the vertical profile (mg m^{-3}). Parameters for eq 13 were provided for nine ranges of chlorophyll-a surface concentrations (Table S2).[30] Data on the surface concentration of chlorophyll-a were obtained from NASA.[34] Below the euphotic zone depth, there is not enough light available to sustain algae growth and the ambient algae concentration was set to zero. The euphotic zone depth was calculated as the depth where 1% of the light present at the ocean surface at noon is still present.[35]

Collisions between algae and microplastic particles were calculated based on existing aggregation theory for formation of marine algal flocs.[36,37] The encounter kernel rate β_A (eq 11) was calculated as the sum of Brownian motion ($\beta_{ABrownian}$), differential settling ($\beta_{Asettling}$), and advective shear (β_{Ashear}) collision frequencies (m^3 s^{-1}). These different encounter kernel rates were calculated as[36,38]

$$\beta_{A_{brownian}} = 4\pi(D_{pl} + D_A)(r_{tot} + r_A)$$

$$\beta_{A_{settling}} = \frac{1}{2}\pi r_{tot}^2 V_s$$

$$\beta_{A_{shear}} = 1.3\gamma(r_{tot} + r_A)^3 \quad (14)$$

in which D_{pl} and D_A are the diffusivity of the plastic particle and the algae cells (m^2 s^{-1}), and γ is the shear rate (s^{-1}). For the Brownian encounter kernel rate, the diffusivity of the plastic and algae was calculated as[36]

$$D_{pl} = \frac{k(T + 273.16)}{6\pi\mu_{sw}r_{tot}} \quad \text{and} \quad D_A = \frac{k(T + 273.16)}{6\pi\mu_{sw}r_A} \quad (15)$$

where k is the Boltzmann constant (m^2 kg s^{-2} K^{-1}), μ_{sw} is the dynamic water viscosity (kg m^{-1} s^{-1}) and where the radius of the total particle, $r_{tot} = r_{pl} + t_{bf}$, and the radius of the algae, r_A, were calculated assuming a spherical particle or algae shape (m).

Algae growth (term 2 in eq 11) was modeled as

$$\mu(T_z, I_z) = \mu_{opt}(I_z)\ \Phi(T_z) \quad \text{for} \quad T_{min} < T_z < T_{max} \quad (16)$$

where $\mu_{opt}(I_z)$ is the growth rate under optimal temperature conditions for a certain light intensity I_z, and $\Phi(T)$ is the temperature influence on the growth rate.[39]

$$\mu_{opt}(I_z) = \mu_{max}\frac{I_z}{I_z + \frac{\mu_{max}}{\alpha}\left(\frac{I_z}{I_{opt}} - 1\right)^2} \quad (17)$$

$$\Phi(T_z) = [(T_z - T_{max})(T_z - T_{min})^2] / [(T_{opt} - T_{min}) \times ((T_{opt} - T_{min})(T_z - T_{opt}) - (T_{opt} - T_{max})(T_{opt} + T_{min} - 2T_z))] \quad (18)$$

In the above equations, I_z is the light intensity at depth z (μE m^{-2} s^{-1}), I_{opt} is the optimal light intensity for algae growth (μE m^{-2} s^{-1}), μ_{max} is the maximum growth rate under optimal conditions (s^{-1}), α is the initial slope (s^{-1}) and T_{max}, T_{min}, and T_{opt} are the maximum, minimum, and optimal temperature to sustain algae growth respectively (°C).[39] For $T_z < T_{min}$ and $T_z > T_{max}$, $\mu_{max} = 0$, and therefore $\mu(T_z,I_z)$ is zero.[39] The light intensity at depth z was calculated according to the law of Lambert−Beer:

$$I_z = I_0\ e^{\epsilon z} \quad (19)$$

in which I_0 is the light intensity at the surface and ϵ is the extinction coefficient (m^{-1}). Light availability at the sea surface was calculated using a sinusoidal function:[40,41]

$$I_0 = I_m \sin(2\pi t) \quad (20)$$

in which I_m is the light intensity at noon (μE m^{-2} s^{-1}). When the sinus function of eq 20 becomes negative, a value of 0 μE m^{-2} s^{-1} was assumed. The light extinction, needed for eq 19, is assumed to be dominated by water and algae induced extinctions, and can be calculated as[40]

$$\epsilon = \epsilon_w + \epsilon_p Chl\ a \quad (21)$$

where ϵ_w and ϵ_p are the extinction coefficients for water and chlorophyll, respectively.

Algae mortality and respiration, that is, terms 3 and 4 of eq 11, respectively, were modeled using a constant mortality and respiration rate. A temperature dependency of respiration was realized with a Q_{10} coefficient. The Q_{10} coefficient indicates how much the respiration rate increases when the temperature increases 10 °C.[42,43] As algae growth (eq 10, term 2) and algae respiration (eq 10, term 4) are temperature dependent, a seawater temperature profile over depth was needed. Seawater temperature was empirically approximated using a Hill function,[44] which adequately captured the characteristic shape of a thermocline:

$$T_z = T_{surf} + (T_{bot} - T_{surf})\frac{z^p}{z^p + z_c^p} \quad (22)$$

in which T_z is the water temperature at depth z (°C), T_{surf} is the water temperature at the surface (°C), T_{bot} is the water temperature at the sea bottom (°C), z_c the thermocline depth (m) and p a parameter defining the steepness of the thermocline.

As mentioned above, the density difference between the particle and seawater is the main driver of the modeled transport. The above eqs 5−22 detailed the calculation of the total particle density (ρ_{tot} in eq 2). Hereafter we focus on the calculation of the seawater density ($\rho_{sw,z}$ in eq 2). Seawater

DOI: 10.1021/acs.est.6b04702
Environ. Sci. Technol. 2017, 51, 7963−7971

density is determined by temperature and salinity (S_z), according to[45]

$$\rho_{sw,z} = (a_1 + a_2T_z + a_3T_z^2 + a_4T_z^3 + a_5T_z^4) + (b_1S_z + b_2S_zT_z + b_3S_zT_z^2 + b_4S_zT_z^3 + b_5S_z^2T_z^2) \quad (23)$$

The temperature profile was calculated with eq 22. A salinity depth profile (S_z, g kg^{-1}) was calculated using a fifth order polynomial function.

$$S_z = c_1z^5 + c_2z^4 + c_3z^3 + c_4z^2 + c_5z + c_6 \quad \text{for} \quad z > z_{fix} \quad (24)$$

Below z_{fix}, the depth at which the salinity profile becomes constant, a constant value S_{fix} is assumed. Last, the kinematic viscosity, $\nu_{sw,z}$ (m^2 s^{-1}), as was used in eq 2, was calculated as

$$\nu_{sw,z} = \frac{\mu_{sw,z}}{\rho_{sw,z}} \quad (25)$$

based on the seawater density and the dynamic viscosity, $\mu_{sw,z}$ (kg m^{-1} s^{-1}). The dynamic viscosity of seawater was calculated using empirical equations.[45] Viscosity was derived from the temperature and salinity profile, by first calculating the water dynamic viscosity $\mu_{w,z}$, followed by calculation of the seawater dynamic viscosity:[45]

$$\mu_{w,z} = 4.2844 \times 10^{-5} + \frac{1}{0.156(T_z + 64.993)^2 - 91.296} \quad (26)$$

$$\mu_{sw,z} = \mu_{w,z}(1 + AS_z + BS_z^2) \quad (27)$$

in which

$$A = 1.541 + 1.998 \times 10^{-2}T_z - 9.52 \times 10^{-5}T_z^2 \quad (28)$$

$$B = 7.974 - 7.561 \times 10^{-2}T_z + 4.724 \times 10^{-4}T_z^2 \quad (29)$$

Parameters and Numerical Model Implementation. Model parameters were estimated based on literature data, and are summarized in Table S1 of the Supporting Information (SI). Here some key choices are briefly discussed. In this model, no specific algae species was modeled. Instead, we modeled an average marine algal species, with the parameter characteristics defined by the mean or median values reported for "marine algae" or "marine phytoplankton". By default, the biofilm density (ρ_{bf}, eq 5) was set at 1388 kg m^{-3}, which is the median of the measured values of Fisher et al. (1983). This median value is of the same order of magnitude as the 1250 kg m^{-3} used in the modeling study by Besseling et al. (2017).[46,47] An algae cell volume (V_A, eq 10) of 2.0 × 10^{-16} m^3 was used, which represents the median value reported by Lopéz-Sandoval et al. (2014).[48] Algae biomass was lost through respiration and mortality (eq 11). In this study a (grazing) mortality of 0.39 d^{-1} was used, a mean value for oceanic habitats.[49] A respiration rate of 0.1 d^{-1} was used in combination with a respiration Q_{10} value of 2, which is a commonly used value.[43,48,50−52] The maximum growth rate (μ_{max}, eq 16) was set at 1.85 d^{-1}, the value reported for *Nannochloropsis oceanica* by Bernard and Rémond (2012).[39] A light intensity at noon of 1.2 × 10^8 μE m^{-2} d^{-1} was used, together with an optimal light intensity of 1.8 × 10^{13} μE m^{-2} d^{-1} (I_m and I_{opt} in eq 20 and 17, respectively).[39,53] A light/dark duration of 12 h each was assumed. The conversion from carbon to algae cells is highly variable, ranging between 35339 to 47.76 pg carbon cell^{-1}.[32] We choose the median value, 2726 × 10^{-9} mg carbon cell^{-1}.

Parameter values for the depth profiles of temperature and salinity were obtained from NASA, choosing the North Pacific near Hawaii as a default location.[54,55] For temperature, eq 22 was fitted through the data points obtained from the surface to 4000 m depth, with a resulting R^2 of 0.99. The salinity profile was fitted as a fifth order polynomial function (R^2 = 0.74) from the surface to 1000 m depth, followed by a constant value from 1000 to 4000 m depth. Parameters of these fits are also provided in Table S1.

The model was solved using MATLAB R2012a with GRIND for MATLAB (http://www.sparcs-center.org/grind.html). Because the modeled system appeared to be a stiff system, the MATLAB's ode23s solver was used.

Model Simulations. Different analyses were done with the model described above, focusing on the effect of particle density and size on vertical transport in the water column. The effect of particle density was studied by simulating the most common polymer types: high density polyethylene (HDPE), low density polyethylene (LDPE), polypropylene (PP), polyvinyl chloride (PVC), and polystyrene (PS). HDPE, LDPE, and PP are initially buoyant plastics (density plastic < density seawater), whereas PVC and PS are nonbuoyant plastics. Together, these polymers account for 87% of the total plastic production of 2007.[56] Properties of these different plastics are summarized in Table S3 of the Supporting Information. To study the effect of size, PP, LDPE, and HDPE particles were simulated with a radius ranging between 10 mm and 0.1 μm. Other simulations focused on the settling onset time and velocity of particles with different densities and sizes.

For several parameters and conditions in the model, values are either variable in the oceans or uncertain. Therefore, we performed scenario analyses where values of key parameters were varied within realistic ranges. For instance, large spatial variability in vertical temperature and density profiles can be observed in the oceans. Therefore, the effect of physical differences among ocean basins on simulation results was assessed. Three locations were simulated for a 0.1 mm LDPE particle, in the North Atlantic near Iceland, in the North Pacific near Hawaii, and in the South Pacific at the latitude of New Zealand and the longitude of Hawaii. These simulations assessed the effect of temperature, salinity, and chlorophyll profiles. The data were obtained from maps of the NASA and the chlorophyll modeling studies (Table S4).[30,33,34,54,55] Furthermore, the effect of biofilm density on the simulation results was assessed for densities of 1100, 1388 (default), and 3000 kg m^{-3}, which resemble realistic densities for marine plankton.[46] Also, simulations were done for a day:night length of 8:16 h and 16:8 h, in addition to the default simulation of 12:12 h, resembling the variability between day and night length throughout the year. Last, the default algae cell volume, V_A in eq 10, was increased and decreased with a factor of 2.

RESULTS AND DISCUSSION

A General Pattern of Buoyant Microplastic Movement in the Ocean. Simulations of initially buoyant and "clean" (nonfouled) microplastics show how biofouling causes the density to increase until particles start to settle (Figure 1). After this initial settling the particles move up again, some of which resurface (Figure 1a) and then continue settling and moving upward again in an oscillatory pattern. Periodicity and

DOI: 10.1021/acs.est.6b04702
Environ. Sci. Technol. 2017, 51, 7963−7971

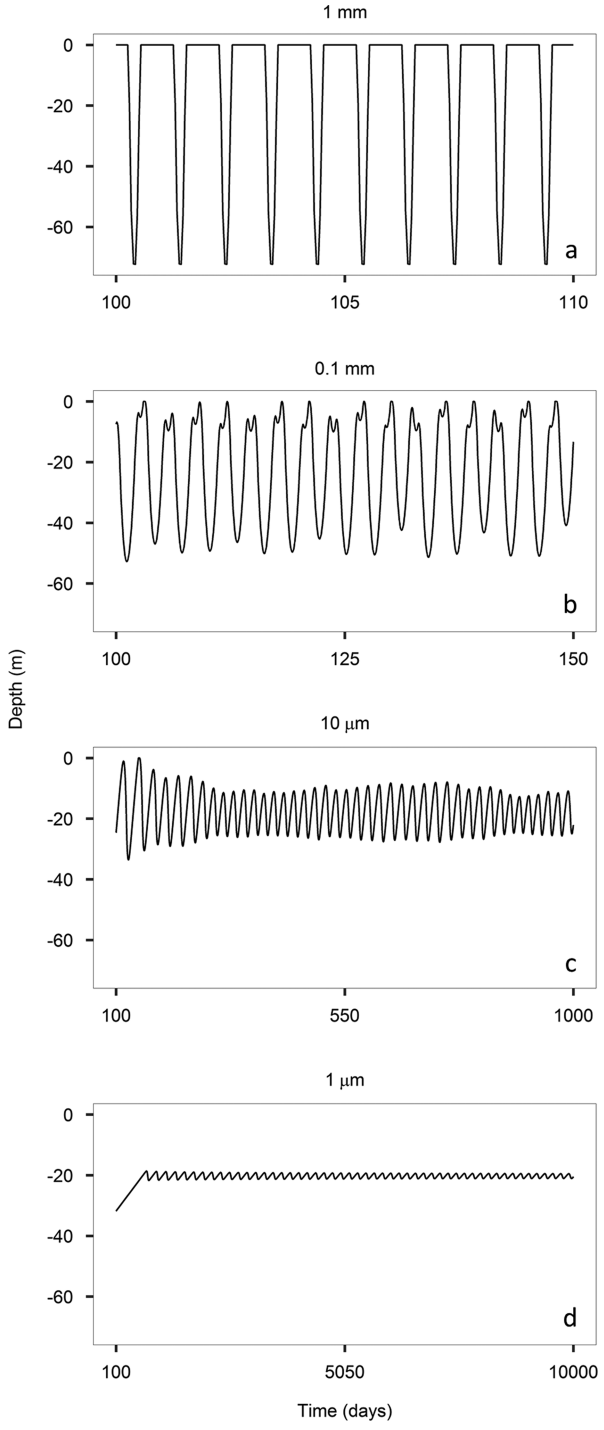

Figure 1. Oscillations of a LDPE particle of (a) 1 mm, (b) 0.1 mm, (c) 10 μm, and (d) 1 μm. Note the different time scales on the x-axis. Oscillation periods increase with decreasing particle size.

amplitude of these oscillations vary with particle size and density and with several other boundary conditions (Figure S1). Below we analyze these model outcomes in detail, by discussing (a) the settling onset time, (b) the settling velocity, (c) the oscillatory patterns and occurrence of chaotic movements, and (d) the effect of parameter variability on the model outcome.

Settling Onset Time of Initially Pristine Microplastics. The settling onset time, that is, the moment particles start settling for the first time, is density and size dependent (Figure 2). The density dependence can be explained as follows. Denser particles settle sooner compared to less dense particles,

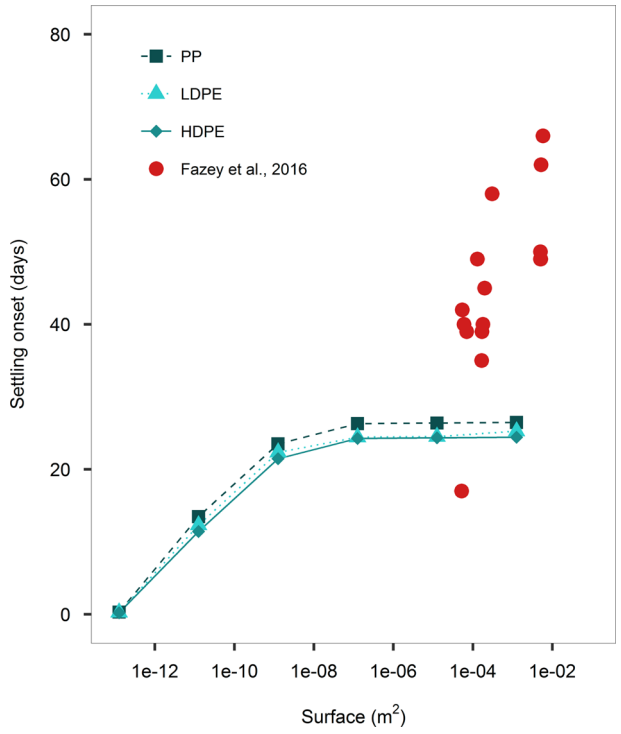

Figure 2. Time needed for a particle of a certain density and surface area to start settling. Denser particles start settling sooner compared to less dense particles when they are of the same size. The effect of particle radius is a trade-off between encounter rates (higher for larger particles) and the surface to volume ratio of the particles (higher for small particles). In red, the results of a field study in Simon's town, South Africa, are shown.[23]

when they are of the same size. When an initially buoyant microplastic particle is denser, less algae of an even higher density are needed to obtain a fouled particle with an overall density that exceeds seawater density. Varying the particle size resulted in an increasing settling onset time with increasing particle size, where the increase levels off when the particles are larger (Figure 2). The mechanism of this effect of particle size can be explained as follows. The settling onset time is a trade-off between the particle's radius and the surface-to-volume ratio. Larger particles have a higher collision frequency with the algae due to shear (eq 14), therefore increasing their density faster compared to smaller particles. The Brownian collision frequency is relatively low compared to the collision frequency due to shear, even for small particles. However, small particles need less algae to start settling, as their surface-to-volume ratio is larger. This trade-off results in the asymptotic shaped relation between the log of the particle surface and the moment at which the particle starts settling for the first time (Figure 2).

Our dynamically modeled theoretical assessment of settling onset time can be compared with empirical data, which however are scarce. For instance, Fazey and Ryan (2016) found that 50% of their square-shaped plastic particles, consisting of HDPE and LDPE which ranged between $5 \times 5 \times 0.1$ mm^3 and $50 \times 50 \times 4$ mm^3 in size, became negatively buoyant between 17 and 62 days in the ocean water.[23] This is in general agreement with our modeling predictions that range from 24 to 26 days for spherical particles with a radius of 1 and 10 mm for

DOI: 10.1021/acs.est.6b04702
Environ. Sci. Technol. 2017, 51, 7963−7971

similar polymer types. Also, Fazey and Ryan (2016)[23] found an increase in the settling onset time with increasing particle surface, which is consistent with our study.

Settling velocity. For initially buoyant microplastics, the settling velocity decreases with decreasing particle size, until a minimal settling velocity is reached (Figure 3). PP particles

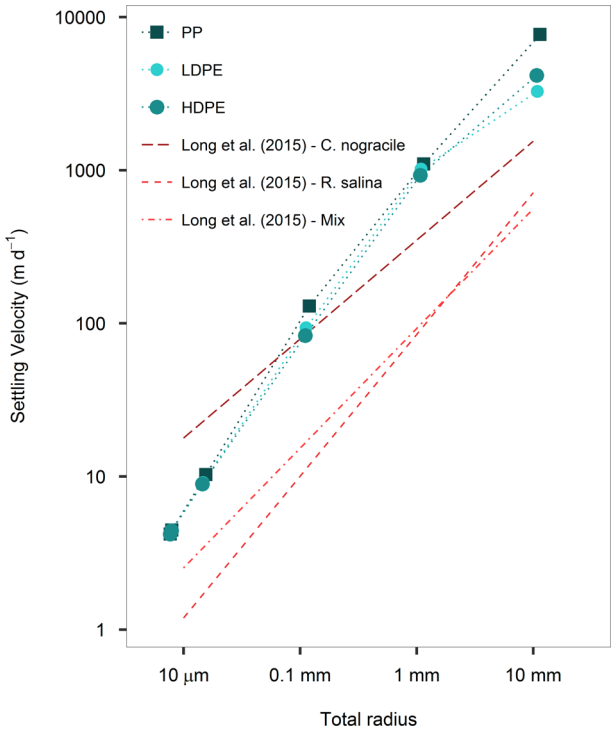

Figure 3. Maximum settling velocity for particles of different sizes and densities. The total radius (x-axis) refers to the radius of the pristine plastic combined with the biofilm, that is, the radius of the aggregate. Pristine particles with a radius of 10, 1, and 0.1 μm have a similar maximum settling velocity, because their total radius is similar after fouling. In red, the empirical equation results of a lab study to phytoplankton aggregates with PS microplastics are shown for different plankton species/compositions.[18]

have a higher settling velocity compared to LDPE and HDPE particles, because the density of a fouled PP particle is larger. As mentioned above, a PP particle needs more time to start settling, as it has to obtain more attached algae to increase its density. Because it needs more algae, the total radius of the fouled particle is higher. Due to this increased size, the encounter rate of the fouled particle with algae also increases, which results in a faster increase of the size and density of a PP particle compared to for example a HDPE particle. Therefore, a PP particle can reach a larger total density, which corresponds with a higher maximum settling velocity. For all particle densities, the maximum settling velocity becomes constant below a certain pristine particle size. This is caused by the difference in algae cell size and plastic particle size. The radius of a single algae cell, assuming a spherical shape, with a volume of 2.0×10^{-16} (Table S1) is 3.6 μm. If we model a particle smaller than 10 μm, the size and density of the fouled particle are defined more by the size of the algae cells than by the size of the plastic particle. Therefore, the size of the fouled particle becomes more or less constant, resulting in a similar settling velocity for these small particles (Figure 3).

Our modeled settling velocities can be compared to empirical data. As mentioned above, Kowalski et al. (2016) verified eq 2, used to calculate the settling velocities for spherical, pristine microplastic particles. They found that the model predicted the settling velocities very well.[25] Long et al. (2015) found that the settling velocity of aggregates containing 2 μm PS particles decreased with a decreasing equivalent spherical diameter.[18] Compared to our model results, their experimental data follow the same trend and the settling velocities are in the same order of magnitude (Figure 3).[18]

In contrast to buoyant particles, microplastics that are denser than water (negatively buoyant), start to settle immediately and sink always to the ocean floor (here modeled at 4000 m depth) (Figure S3). The time to sink to the ocean floor is particle size and density dependent. Larger particles settle faster: a particle of 10 mm needs only 1.6 (PVC) or 23 (PS) minutes to sink 4000 m, whereas a 0.1 mm particle already needs 10 (PVC) or 159 (PS) days to sink this distance, and a 1 μm particle needs 278 (PVC) or 4317 (PS) years to finally end on the ocean floor (Figure S3). Because plastic production started in the 1950s,[57] it can be assumed that nonbuoyant particles smaller than 10 μm have not been able to reach the ocean floor yet. In fact, because of their very slow transport, these smaller particles can be anywhere in the water column. As seawater density is dependent on temperature and salinity (eq 23), there is no fixed polymer density threshold at which particles end on the ocean floor. A study on microplastics in deep sea sediments indicated that most particles found were denser than seawater,[22] which is in general agreement with our modeling results.

Oscillations and Chaotic Behavior. Simulations of initially clean buoyant microplastics showed how biofouling caused their density to increase until the particles started to settle (Figures 1 and 2). After this initial settling, buoyant particles never settle to a fixed water level, but keep moving up and down in the water column (Figure 1). Sinking, rising, and oscillations are explained by the dynamics of the differences between the density of the seawater and the plastic particle. At the moments where particle and seawater density are equal, the settling velocity (eq 1) is zero. The density oscillation curve has inflection points, which coincide exactly with the minima and maxima in the depth oscillation curve, where the direction of vertical transport is reversed (Figure S2). If the particle density exceeds seawater density it will sink, whereas it will rise or float at the surface. Density differences are explained by the biofilm thickness, which in turn is explained by the biofilm volume, and thus by the number of algae. The number of algae on the particle surface is explained by collision, growth, mortality, and respiration. The interaction of these different growth and loss processes determines whether a particle sinks or moves upward again. The external forcing of light variation at the surface together with the depth profiles of light extinction, salinity, density, viscosity, and chlorophyll, in turn influence the algae collision, growth, respiration, and settling velocity.

Some oscillations display a fixed daily period, such as the 1 mm LDPE particle which reaches a maximum depth every 24 h (Figure 1a). These maximum depths are reached around noon, because algae growth is enhanced by the light intensity. During the night, respiration takes over and the particle resurfaces and stays at the surface until the light reappears and the biofilm has grown enough to start settling again. Circadian cycles, or 24 h cycles, have been observed in algal behavior, where an increase in chlorophyll-a concentrations is observed during the day,

DOI: 10.1021/acs.est.6b04702
Environ. Sci. Technol. 2017, 51, 7963−7971

while a decrease is found during dark hours.[58−60] The circadian cycles observed in algal growth can be considered a good proxy for biofilm driven microplastic circadian cycles as simulated in this study (Figure 1a, Figure S1).

However, not all simulated oscillations display a daily period. For example, the simulated 0.1 mm particle reaches its minimum around every 3 days, and the 10 μm particle only reaches its minimum around every 21 days (Figure 1 panels b and c, respectively). As some of these oscillations were complicated, we tested for deterministic chaos in these simulations. Deterministic chaos is defined as "aperiodic long-term behaviour in a deterministic system that exhibits sensitive dependence on initial conditions".[61] Our model indeed is deterministic as no random factors are included and it shows aperiodic long-term behavior. In the case of chaos, the trajectories are fundamentally unpredictable due to the sensitivity to the initial condition. The Lyapunov exponent is a measure for chaos, as it indicates this sensitivity by showing the difference between two simulations with slightly different initial conditions.[61] Lyapunov exponents were calculated for different plastic types and sizes. For our standard scenario's (PP, LDPE, and HDPE with radii ranging between 10 mm and 0.1 μm) no chaos was found (Table S5). A systematic assessment of chaotic behavior of the modeled system for all parameter values was beyond the scope of this paper.

Oscillation periods and amplitudes not only differ for different plastic densities and sizes, but also depend on other parameters. Varying all parameter values was beyond the scope of this study, instead we focused on the key parameters affecting the particle growth and density. The dependence of the settling dynamics on the biofilm density (eq 5) was studied for three different densities. With increasing biofilm density, the settling onset time decreased (Figure S4). As each individual algae cell aggregating with the microplastic particle has a higher mass, the mass of the aggregate increases more rapidly, resulting in a decrease in the settling onset. Oscillation amplitudes tend to increase with increasing biofilm density, and are variable within each scenario. The day/night duration affected the particle settling too (eq 2). With an 8 h light and 16 dark regime, settling only occurred after more than 116 days. With increasing light duration, algae growth was enhanced, and the settling onset time decreased (Figure S5). The algae cell volume (eq 10) affects the settling onset time too, which increased with decreasing cell volume (Figure S6). The amplitude of the settling oscillations remained similar under different light durations and algae cell volumes.

Oceanographic Zones and Wind Mixing. For LDPE particles of 0.1 mm, particle sinking behavior was assessed for different oceanic conditions, representing different oceanographic zones (Table S4). Differences in temperature, salinity, algae surface concentrations, and thermocline depth affected the model outcome of the LDPE particles. Interestingly, settling only started within 100 days for the North Pacific scenario (Figure S7). For the South Pacific scenario, settling started after 700 days. Although chlorophyll concentrations were higher in the North Atlantic, particles did not settle. This is the result of the low temperatures, which hamper algae growth. Here we emphasize that many other parameters vary in the ocean, such as biofouling seasonality,[62] spatial variability in light extinction,[63] algae adaptations to temperature,[64] and the daily sunshine duration. However, varying all these parameters was beyond the scope of this first theoretical study.

Another process which was beyond the scope of this study is the effect of wind mixing and turbulent flow on the settling. Our model is designed for relatively quiescent conditions. In the case of more turbulent surface conditions and increased wind mixing, plastic debris is found to be vertically distributed in the upper part of the water column (the ocean surface mixed layer, OSML).[14,65−68] Wind mixing results in an exponential decrease in particle concentrations with depth, the extent of the decrease being inversely proportional to wind speed.[14,65−68] If particles would be held in the OSML and shielded from light, a delay in the modeled onset of settling would occur until quiescent conditions are re-established. If particles would not be shielded from light, biofilm growth would be further enhanced because of the optimal conditions for algae growth (light, temperature) in the OSML. We can assume, however, that particles will not be effectively held in the OSML. After all, it has been found that the mixed layer is only 0−5 m thick[14,66] and this is not deep enough to attenuate light penetration and limit biofouling. Particles will still grow a biofilm and escape the OSML after which they settle and oscillate according to the simulations presented here.

General Discussion. The main objective of this study was to simulate the sinking of microplastics when fouled, using a theoretical model. Because concentration profiles over 100 m (buoyant microplastics) or 4000 m depth (nonbuoyant microplastics) are not available for the oceans, no formal model validation against measurement data is possible. The model should be considered as a theoretical tool that can be used for prospective exposure assessments or for evaluating hypotheses regarding the fate of microplastic in the oceans. Nevertheless, general features of the modeled profiles can be discussed against patterns reported in the literature.

A size-selective removal of particles at the ocean surface was observed by Cozar et al. (2014).[6] They found an increasing amount of smaller particles at the ocean surface, up to a threshold value of 2 mm in size. Particle abundance of 1 mm and smaller decreased at the sea surface with decreasing particle size.[6,11] Our model predicts that all particles can settle due to biofouling, and larger particles start settling last. Because of this late settling onset, particles are present longer at the ocean surface. Also, larger particles, such as 10 mm and 1 mm particles, oscillate at a fast rate and resurface with each oscillation. Smaller particles, from 10 μm onward, do not resurface anymore. Over time, this therefore results in a size selective removal of smaller particles from the surface, which is in general agreement with the observations by Cozar et al. (2014).[6] Also, the settling onset time and settling velocities modeled in this study correspond to those observed in field studies (Figures 2 and 3).[18,23] Considering the consistency among the data and our model simulations, biofouling could therefore be a valid hypothesis explaining the size-selective removal of small particles at the ocean surface. Other processes, such as marine snow formation, could further enhance the settling of initially buoyant plastics. Marine snow, aggregates consisting of a mixture of organic materials, is not depending on light for its formation. Therefore, it could be an additional mechanism to explain the observed size-selective removal of microplastics and a potential pathway for microplastics to reach to ocean floor.[69,70]

Buoyant particles are calculated to sink and oscillate below the ocean surface. We showed that nanosized particles, that is, those smaller than 10 μm, sink so slowly that they can reside anywhere in the water column. Also, we demonstrated that

DOI: 10.1021/acs.est.6b04702
Environ. Sci. Technol. 2017, 51, 7963−7971

different plastic and biofilm properties, together with oceanographic conditions, result in a different particle fate. If the model represents reality, this has important implications for the type of exposure and risks of plastic debris on the ocean floor versus that in the water column. Because emission of plastic to sea is predicted to increase by orders of magnitude[1] and nanofragmentation is generally believed to continuously convert debris to this <1 μm size class,[71] we hypothesize that the water column may eventually host a uniform dispersion of nanoplastic particles. Hence, further development and validation of plastic biofouling−nanofragmentation models is to be recommended.

■ ASSOCIATED CONTENT

Supporting Information

The Supporting Information is available free of charge on the ACS Publications website at DOI: 10.1021/acs.est.6b04702.

Text, figures, and tables address the (a) nomenclature, (b) plastic characteristics and environmental transect data, and (c) figures of oscillations for different plastic types, the relation between particle density and settling, oscillation figures for different environmental conditions and results of the chaos analysis (PDF)

■ AUTHOR INFORMATION

Corresponding Author

*E-mail: merel.kooi@wur.nl.

ORCID

Merel Kooi: 0000-0003-0092-5209

Albert A. Koelmans: 0000-0001-7176-4356

Notes

The authors declare no competing financial interest.

■ REFERENCES

(1) Jambeck, J. R.; Geyer, R.; Wilcox, C.; Siegler, T. R.; Perryman, M.; Andrady, A.; Narayan, R.; Law, K. L. Plastic waste input from land into the ocean. *Science (Washington, DC, U. S.)* **2015**, *347* (6223), 768−771.

(2) Browne, M. A.; Galloway, T.; Thompson, R. Microplastics - An emerging contaminant of potential concern? *Integr. Environ. Assess. Manage.* **2007**, *3* (4), 559−566.

(3) Morét-Ferguson, S.; Law, K. L.; Proskurowski, G.; Murphy, E. K.; Peacock, E. E.; Reddy, C. M. The size, mass, and composition of plastic debris in the western North Atlantic Ocean. *Mar. Pollut. Bull.* **2010**, *60* (10), 1873−1878.

(4) Doyle, M. J.; Watson, W.; Bowlin, N. M.; Sheavly, S. B. Plastic particles in coastal pelagic ecosystems of the Northeast Pacific ocean. *Mar. Environ. Res.* **2011**, *71* (1), 41−52.

(5) Hidalgo-ruz, V.; Gutow, L.; Thompson, R. C.; Thiel, M. Microplastics in the Marine Environment: A Review of the Methods Used for Identification and Quantification. *Environ. Sci. Technol.* **2012**, *46* (6), 3060−3075.

(6) Cózar, A.; Echevarría, F.; González-Gordillo, J. I.; Irigoien, X.; Ubeda, B.; Hernández-León, S.; Palma, A. T.; Navarro, S.; García-de-Lomas, J.; Ruiz, A.; et al. Plastic debris in the open ocean. *Proc. Natl. Acad. Sci. U. S. A.* **2014**, *111*, 10239−10244.

(7) Wright, S. L.; Thompson, R. C.; Galloway, T. S. The physical impacts of microplastics on marine organisms: A review. *Environ. Pollut.* **2013**, *178*, 483−492.

(8) Setälä, O.; Fleming-Lehtinen, V.; Lehtiniemi, M. Ingestion and transfer of microplastics in the planktonic food web. *Environ. Pollut.* **2014**, *185*, 77−83.

(9) Foekema, E. M.; De Gruijter, C.; Mergia, M. T.; van Franeker, J. A.; Murk, A. J.; Koelmans, A. A. Plastic in north sea fish. *Environ. Sci. Technol.* **2013**, *47* (15), 8818−8824.

(10) Besseling, E.; Wegner, A.; Foekema, E. M.; Van Den Heuvel-Greve, M. J.; Koelmans, A. A. Effects of microplastic on fitness and PCB bioaccumulation by the lugworm Arenicola marina (L.). *Environ. Sci. Technol.* **2012**, *47* (1), 593−600.

(11) Eriksen, M.; Lebreton, L. C. M.; Carson, H. S.; Thiel, M.; Moore, C. J.; Borerro, J. C.; Galgani, F.; Ryan, P. G.; Reisser, J. Plastic Pollution in the World's Oceans: More than 5 Trillion Plastic Pieces Weighing over 250,000 Tons Afloat at Sea. *PLoS One* **2014**, *9* (12), e111913.

(12) Thompson, R. C.; Olsen, Y.; Mitchell, R. P.; Davis, A.; Rowland, S. J.; John, A. W. G.; McGonigle, D.; Russell, A. E. Lost at sea: where is all the plastic? *Science* **2004**, *304* (5672), 838.

(13) Law, K. L.; Morét-Ferguson, S.; Maximenko, N. A.; Proskurowski, G.; Peacock, E. E.; Hafner, J.; Reddy, C. M. Plastic accumulation in the North Atlantic subtropical gyre. *Science (Washington, DC, U. S.)* **2010**, *329* (5996), 1185−1188.

(14) Reisser, J.; Slat, B.; Noble, K.; Du Plessis, K.; Epp, M.; Proietti, M.; De Sonneville, J.; Becker, T.; Pattiaratchi, C. The vertical distribution of buoyant plastics at sea: An observational study in the North Atlantic Gyre. *Biogeosciences* **2015**, *12* (4), 1249−1256.

(15) Ye, S.; Andrady, A. L. Fouling of floating plastic debris under Biscayne Bay exposure conditions. *Mar. Pollut. Bull.* **1991**, *22* (12), 608−613.

(16) Lattin, G. L.; Moore, C. J.; Zellers, a. F.; Moore, S. L.; Weisberg, S. B. A comparison of neustonic plastic and zooplankton at different depths near the southern California shore. *Mar. Pollut. Bull.* **2004**, *49* (4), 291−294.

(17) Lobelle, D.; Cunliffe, M. Early microbial biofilm formation on marine plastic debris. *Mar. Pollut. Bull.* **2011**, *62* (1), 197−200.

(18) Long, M.; Moriceau, B.; Gallinari, M.; Lambert, C.; Huvet, A.; Raffray, J.; Soudant, P. Interactions between microplastics and phytoplankton aggregates: Impact on their respective fates. *Mar. Chem.* **2015**, *175*, 39−46.

(19) Zardus, J. D.; Nedved, B. T.; Huang, Y.; Tran, C.; Hadfield, M. G. Microbial biofilms facilitate adhesion in biofouling invertebrates. *Biol. Bull.* **2008**, *214* (1), 91−98.

(20) Bergmann, M.; Klages, M. Increase of litter at the Arctic deep-sea observatory HAUSGARTEN. *Mar. Pollut. Bull.* **2012**, *64* (12), 2734−2741.

(21) Van Cauwenberghe, L.; Vanreusel, A.; Mees, J.; Janssen, C. R. Microplastic pollution in deep-sea sediments. *Environ. Pollut.* **2013**, *182*, 495−499.

(22) Woodall, L. C.; Sanchez-Vidal, A.; Canals, M.; Paterson, G. L. J.; Coppock, R.; Sleight, V.; Calafat, A.; Rogers, A. D.; Narayanaswamy, B. E.; Thompson, R. C. The deep sea is a major sink for microplastic debris. *R. Soc. Open Sci.* **2014**, *1* (4), 140317.

(23) Fazey, F. M. C.; Ryan, P. G. Biofouling on buoyant marine plastics: An experimental study into the effect of size on surface longevity. *Environ. Pollut.* **2016**, *210*, 354−360.

(24) Dietrich, W. E. Settling velocity of natural particles. *Water Resour. Res.* **1982**, *18* (6), 1615−1626.

(25) Kowalski, N.; Reichardt, A. M.; Waniek, J. J. Sinking rates of microplastics and potential implications of their alteration by physical, biological, and chemical factors. *Mar. Pollut. Bull.* **2016**, *109* (1), 310−319.

(26) Carson, H. S.; Nerheim, M. S.; Carroll, K. A.; Eriksen, M. The plastic-associated microorganisms of the North Pacific Gyre. *Mar. Pollut. Bull.* **2013**, *75* (1−2), 126−132.

(27) Kiørboe, T.; Tang, K.; Grossart, H. P.; Ploug, H. Dynamics of microbial communities on marine snow aggregates: Colonization, growth, detachment, and grazing mortality of attached bacteria. *Appl. Environ. Microbiol.* **2003**, *69* (6), 3036−3047.

(28) James, S. C.; Boriah, V. Modeling algae growth in an open-channel raceway. *J. Comput. Biol.* **2010**, *17* (7), 895−906.

(29) Béchet, Q.; Shilton, A.; Guieysse, B. Modeling the effects of light and temperature on algae growth: State of the art and critical

DOI: 10.1021/acs.est.6b04702
Environ. Sci. Technol. 2017, 51, 7963−7971

assessment for productivity prediction during outdoor cultivation. *Biotechnol. Adv.* **2013**, *31* (8), 1648−1663.
(30) Uitz, J.; Claustre, H.; Morel, A.; Hooker, S. B. Vertical distribution of phytoplankton communities in open ocean: An assessment based on surface chlorophyll. *J. Geophys. Res.* **2006**, *111*, C8.
(31) Cloern, J. E.; Grenz, C.; Vidergar-Lucas, L. An empirical model of the phytoplankton chlorophyll: carbon ratio-the conversion factor between productivity and growth rate. *Limnol. Oceanogr.* **1995**, *40* (7), 1313−1321.
(32) Menden-Deuer, S.; Lessard, E. J. Carbon to volume relationships for dinoflagellates, diatoms, and other protist plankton. *Limnol. Oceanogr.* **2000**, *45* (3), 569−579.
(33) Ardyna, M.; Babin, M.; Gosselin, M.; Devred, E.; Bélanger, S.; Matsuoka, A.; Tremblay, J.-É. Parameterization of vertical chlorophyll a in the Arctic Ocean: impact of the subsurface chlorophyll maximum on regional, seasonal, and annual primary production estimates. *Biogeosciences* **2013**, *10* (6), 4383.
(34) NASA. Chlorophyll concentration. http://neo.sci.gsfc.nasa.gov/view.php?datasetId=MY1DMM_CHLORA&year=2014 (accessed Sep 16, 2015).
(35) Kirk, J. T. O. *Light and Photosynthesis in Aquatic Ecosystems*; Cambridge University Press, 1994.
(36) Jackson, G. A. A model of the formation of marine algal flocs by physical coagulation processes. *Deep-Sea Res., Part A* **1990**, *37* (8), 1197−1211.
(37) Burd, A. B.; Jackson, G. A. Particle aggregation. *Annu. Rev. Mar. Sci.* **2009**, *1*, 65−90.
(38) Farley, K. J.; Morel, F. M. M. Role of coagulation in the kinetics of sedimentation. *Environ. Sci. Technol.* **1986**, *20* (2), 187−195.
(39) Bernard, O.; Rémond, B. Validation of a simple model accounting for light and temperature effect on microalgal growth. *Bioresour. Technol.* **2012**, *123*, 520−527.
(40) Robson, B. J. Representing the effects of diurnal variations in light on primary production on a seasonal time-scale. *Ecol. Modell.* **2005**, *186* (3), 358−365.
(41) Bonnefond, H.; Moelants, N.; Talec, A.; Bernard, O.; Sciandra, A. Concomitant effects of light and temperature diel variations on the growth rate and lipid production of Dunaliella salina. *Algal Res.* **2016**, *14*, 72−78.
(42) Edwards, K. F.; Thomas, M. K.; Klausmeier, C. A.; Litchman, E. Phytoplankton growth and the interaction of light and temperature: A synthesis at the species and community level. *Limnol. Oceanogr.* **2016**, *61* (4), 1232−1244.
(43) Eppley, R. W. Temperature and phytoplankton growth in the sea. *Fish. Bull.* **1972**, *70* (4), 1063−1085.
(44) Hill, A. V. The possible effects of the aggregation of the molecules of haemoglobin on its dissociation curves. *J. Physiol* **1910**, *40*, 4−7.
(45) Sharqawy, M. H.; Lienhard, V.; Zubair, J. H. S. M. Thermophysical properties of seawater: a review of existing correlations and data. *Desalin. Water Treat.* **2010**, *16*, 354−380.
(46) Fisher, N. S.; Bjerregaard, P.; Fowler, S. W. Interactions of marine plankton with transuranic elements. I. Biokinetics of neptunium, plutonium. americium and californium in phytoplankton. *Limnol. Oceanogr.* **1983**, *28* (3), 432−447.
(47) Besseling, E.; Quik, J. T. K.; Sun, M.; Koelmans, A. A. Fate of nano- and microplastic in freshwater systems: a modeling study. *Environ. Pollut.* **2017**, *220*, 540−548.
(48) López-Sandoval, D. C.; Rodriguez-Ramos, T.; Cermeño, P.; Sobrino, C.; Marañón, E. Photosynthesis and respiration in marine phytoplankton: relationship with cell size, taxonomic affiliation, and growth phase. *J. Exp. Mar. Biol. Ecol.* **2014**, *457*, 151−159.
(49) Calbet, A.; Landry, M. R.; et al. Phytoplankton growth, microzooplankton grazing, and carbon cycling in marine systems. *Limnol. Oceanogr.* **2004**, *49* (1), 51−57.
(50) Ras, M.; Steyer, J.-P.; Bernard, O. Temperature effect on microalgae: a crucial factor for outdoor production. *Rev. Environ. Sci. Bio/Technol.* **2013**, *12* (2), 153−164.
(51) Miller, L. P.; Allen, B. J.; King, F. A.; Chilin, D. R.; Reynoso, V. M.; Denny, M. W. Warm microhabitats drive both increased respiration and growth rates of intertidal consumers. *Mar. Ecol.: Prog. Ser.* **2015**, *522*, 127−143.
(52) Montagnes, D. J. S.; Kimmance, S. A.; Atkinson, D. Using Q10: can growth rates increase linearly with temperature? *Aquat. Microb. Ecol.* **2003**, *32* (3), 307−313.
(53) Klausmeier, C. A.; Litchman, E. Algal games: The vertical distribution of phytoplankton in poorly mixed water columns. *Limnol. Oceanogr.* **2001**, *46* (8), 1998−2007.
(54) Locarnini, R. A.; Mishonov, A. V.; Antonov, J. I.; Boyer, T. P.; Garcia, H. E.; Baranova, O. K.; Zweng, M. M.; Paver, C. R.; Reagan, J. R.; Johnson, D. R.; et al. World Ocean Atlas 2013. Vol. 1: Temperature. *A. Mishonov, Technol. Ed. NOAA Atlas NESDIS* **2013**, *73*, 40.
(55) Zweng, M. M.; Reagan, J. R.; Antonov, J. I.; Locarnini, R. A.; Mishonov, A. V.; Boyer, T. P.; Garcia, H. E.; Baranova, O. K.; Johnson, D. R.; Seidov, D.; et al. World Ocean Atlas 2013. Vol. 2: Salinity. *NOAA Atlas NESDIS* **2013**, *74*, 39.
(56) Andrady, A. L. Microplastics in the marine environment. *Mar. Pollut. Bull.* **2011**, *62* (8), 1596−1605.
(57) *Plastics—The Facts*; PlasticEurope, 2010.
(58) Ditty, J. L.; Williams, S. B.; Golden, S. S. A cyanobacterial circadian timing mechanism. *Annu. Rev. Genet.* **2003**, *37* (1), 513−543.
(59) Blanken, W.; Magalhães, A.; Sebestyén, P.; Rinzema, A.; Wijffels, R. H.; Janssen, M. Microalgal biofilm growth under day-night cycles. *Algal Res.* **2017**, *21*, 16−26.
(60) Post, A. F.; Dubinsky, Z.; Wyman, K.; Falkowski, P. G. Kinetics of light-intensity adaptation in a marine planktonic diatom. *Mar. Biol.* **1984**, *83* (3), 231−238.
(61) Strogatz, S. H. *Nonlinear Dynamics and Chaos: With Applications to Physics, Biology, Chemistry, And Engineering*; Westview Press, 2014.
(62) Artham, T.; Sudhakar, M.; Venkatesan, R.; Madhavan Nair, C.; Murty, K. V. G. K.; Doble, M. Biofouling and stability of synthetic polymers in sea water. *Int. Biodeterior. Biodegrad.* **2009**, *63* (7), 884−890.
(63) Lorenzen, C. J. Extinction of light in the ocean by phytoplankton. *ICES J. Mar. Sci.* **1972**, *34* (2), 262−267.
(64) Nielsen, E. S.; Jørgensen, E. G. The adaptation of plankton algae. *Physiol. Plant.* **1968**, *21* (3), 647−654.
(65) Kukulka, T.; Proskurowski, G.; Morét-Ferguson, S.; Meyer, D. W.; Law, K. L. The effect of wind mixing on the vertical distribution of buoyant plastic debris. *Geophys. Res. Lett.* **2012**, *39* (7), 1−6.
(66) Kooi, M.; Reisser, J.; Slat, B.; Ferrari, F. F.; Schmid, M. S.; Cunsolo, S.; Brambini, R.; Noble, K.; Sirks, L.-A.; Linders, T. E. W.; Schoeneich-Argent, R. I.; Koelmans, A. A. The effect of particle properties on the depth profile of buoyant plastics in the ocean. *Sci. Rep.* **2016**, *6*, 6.
(67) Kukulka, T.; Brunner, K. Passive buoyant tracers in the ocea surface boundary layer: 1. Influence of equilibirum wind-waves on vertical distributions. *J. Geophys. Res. Ocean.* **2015**, *120*, 1−16.
(68) Brunner, K.; Kukulka, T.; Proskurowski, G.; Law, K. L. Passive buoyant tracers in the ocean surface boundary layer: II. Observations and simulations of microplastic marine debris. *J. Geophys. Res. Ocean* **2015**, *120*, 7559.
(69) Asper, V. L. Measuring the flux and sinking speed of marine snow aggregates. *Deep-Sea Res., Part A* **1987**, *34* (1), 1−17.
(70) Shanks, A. L.; Trent, J. D. Marine snow: sinking rates and potential role in vertical flux. *Deep-Sea Res., Part A* **1980**, *27* (2), 137−143.
(71) Koelmans, A. A.; Diepens, N. J.; Velzeboer, I.; Besseling, E.; Quik, J. T. K.; van de Meent, D. Guidance for the prognostic risk assessment of nanomaterials in aquatic ecosystems. *Sci. Total Environ.* **2015**, *535*, 141−149.

DOI: 10.1021/acs.est.6b04702
Environ. Sci. Technol. 2017, 51, 7963−7971